A High-Speed Electro-Optic Modulator with Optimized Electrode Positions

Hany Mahrous[1], Michael Gad[2], Mona El Sabbagh[2], Mostafa Fedawy[1], W. Fikry[2]

(1): Electronics and Communications Department, Faculty of Engineering, Arab Academy for Science and Technology and Maritime Transport, Egypt.
(2): Engineering Physics and Mathematics Department, Faculty of Engineering, Ain Shams University, Cairo, Egypt

h.a.mahmod@gmail.com, mmonirmo@eng.asu.edu.eg, mona.mohammed@eng.asu.edu.eg, m.fedawy@aast.edu, wael_fikry@eng.asu.edu.eg

***Abstract*—A metal-oxide-semiconductor electro-optic modulator is proposed. The modulator is based on silicon-on-insulator technology. The metallic electrodes are positioned in order to minimize the optical absorption losses. This results in the advantages of very small insertion loss of 5.4 dB and very high extinction ratio of 28 dB. Moreover, the modulator design enables future simple fabrication with only one doping mask. The modulator exhibits a very high speed of operation of 100 GHz. The other features of this modulator, such as the size and operating voltage are competitive to other modulators of the same category.**

Keywords—integrated optics; silicon photonics; photonic devices; electro-optic modulators.

I. INTRODUCTION

Integrated optics continues to attract a lot of research work in many directions such as biomedical applications [1], gas sensing [2] and telecommunications systems [3]. At the heart of any optical telecommunications system lies the electro-optic modulator [4-5]. This is a device that loads the electronic data to a laser carrier. Using a modulator, many channels of tremendous data can be loaded to an optical channel. Then, using multiplexers, the channels can be then multiplexed and sent over optical fiber links for long distances with typical losses of 0.2 dB/km [6] and very small dispersion. This high bandwidth transmission is the main attraction of photonics circuits.

In order to implement integrated optical devices and circuits, silicon on insulator (SOI) technology was introduced amongst other platforms. However, since SOI possesses the upper hand in the electronics industry, special attention was directed toward manipulating this technology to produce integrated optical circuits. The objective is to enable monolithic integration of photonic circuits with the well-established electronic circuits so that hybrid systems with super performance features can be realized [7].

From the optical point of view, the silicon-on-silica platform enjoys a strong refractive index contrast of approximately 2 at the C-band communications wavelength λ_o=1.55 μm. This contrast makes possible for light to go around arcs of small radii [8]. Therefore, photonic circuits can be integrated with high density. Moreover, at wavelength λ_o=1.55 μm, silicon and silica are transparent. This platform was successfully utilized to fabricate basic circuits such as ring resonators, interleavers [9], sensors [10], gyroscopes and fiber-grating couplers [11].

On the other hand, silicon exhibits a poor electro-optic coefficient [12] and therefore cannot be used as an electro-optic modulator by simply applying a potential difference across it. Besides, despite the fact that its thermo-optic coefficient is relatively good, thermal modulation is very limited in speed [13].

The solutions suggested to get around this problem are many. One solution is to utilize a high electro-optic coefficient material, such as certain polymers. This material serves as cladding to a silicon waveguide. The overlap between the mode power and this cladding enables the modulation of the propagating mode [5]. However, with the high refractive index of silicon, compared to such materials, the mode confinement factor, i.e. the portion of the mode power contained in the core, is large and a small portion of the mode power overlaps with the cladding. The other solution, which has been very successful so far, is to use plasma injection and/or extraction [14]. In this solution, free carriers, electrons and/or holes, can be injected into the core of the waveguide to decrease its refractive index, while increasing the laser absorption loss, or be extracted to do the contrary. Therefore, plasma based modulators can be sorted in two main groups. First, the injection based modulators which usually feature a stronger refractive index variation and hence a smaller modulator length and operating voltage. On the other hand, those modulators suffer from an electrical direct current (DC) loss besides a larger optical absorption loss and consequently a higher insertion loss and a lower extinction ratio. Moreover, those modulators show much smaller bandwidth, obviously because of the carrier life time limitations. Second, the depletion based modulators represent the contrast, and became the most favorable, no wonder because of their high speed of operation, zero DC electrical losses and low optical losses. Two other mechanisms, charge accumulation and inversion were also utilized for modulation [15], but without as much attention. Like depletion, no excess charge is introduced to the silicon waveguide but rather there is a redistribution of the

pre-existing charge in order to create a change to the refractive index.

Many modulator configurations were proposed so far and noticeably, while aiming at increasing the interaction between the laser power and the free carriers or the depletion layer, these modulators are getting more and more complicated in terms of doping profiles and silicon layer geometry [4]. Such complications make the practical realization of such modulators very challenging.

In this work, we revert to the initial simple idea of the metal-oxide-semiconductor (MOS) capacitor, taking one step forward by optimizing the metallic electrode position, with respect to the core of the waveguide, in order to minimize the interaction between the electrode and the propagating mode, and hence minimizing the absorption losses. Yet, the electrodes are placed close enough to the core to produce a strong change in the refractive index. The approach here stresses on the manufacturability of the modulator by minimizing the number of required masks and simplifying the geometry. This qualifies the modulator for future fabrication through relatively inexpensive multi-project-wafer (MPW) prototyping, like the one offered by IMEC, for example shown in [9]. The objective is also that the device features a high speed of operation with the smallest possible footprint and minimum losses. The simulations were carried using DEVICE (version 7.2.1634), for the charge transport part, and MODE (version 7.12.1634), for the optical modal analysis part, both from Lumerical [16].

II. Modulator Structure and Performance Metrics

The cross section of the modulator is illustrated in Fig. 1. The device comprises a strip waveguide and two golden electrodes. The waveguide has a silicon core of rectangular cross section of height H and width W. One electrode is placed to the right of the waveguide and another to the left. Elsewhere, silica exists. The dimensions of any electrode are taken similar to those of the waveguide. The waveguide core is doped with acceptors of concentration $p=10^{17}$ cm^{-3}. The optical mode propagates in the direction normal to this cross section.

As shown in Fig. 1, the vertical distance between the lower edge of the waveguide and the lower edge of any electrode is denoted by 'z_o'. This way, $z_o = 0$, means that the electrode is just beside the waveguide with no vertical misalignment. When $z_o > 0$, we mean that the right electrode is moved up and the left electrode is moved down by the same distance 'z_o'. The horizontal separation, measured between the right edge of the waveguide and the left side of the right electrode, is denoted by 'y_o'. The left electrode is separated from the waveguide by the same distance, measured between the left edge of the waveguide and the right of the electrode. In other words, the structure is symmetric about the center of the waveguide core.

The operating wavelength is λ_o = 1.55 µm and the corresponding optical constants of the three materials in this structure are taken as the default values in MODE which are taken from Palik [17]. The electrical properties are taken from Sze [18].

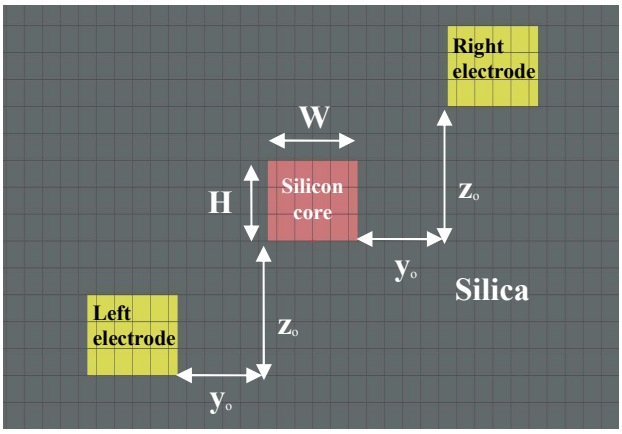

Fig. 1.The modulator cross section. The two electrodes have dimensions similar to the silicon core.

Before getting into detailed results, the metrics of the modulator performance should be reviewed [4]. These metrics usually are referred to a symmetric Mach-Zender Interferometer (MZI) based modulator [4], [13]. The length of any arm of the MZI is L. The voltage required to fully switch between maximum and minimum output optical power is V_π. This voltage can be applied to one arm of the MZI or distributed between the two arms (push-pull technique). The output power switching depends on the phase difference between the two arms. If the waves propagating in the two arms are in phase, the output is maximum. If they are completely out of phase, i.e. the phase difference between the waves is π, then the output is minimum. The switching voltage is responsible for this phase difference between the two arms. This is achieved through changing the charge distribution, and consequently the effective refractive index, n_e, of the propagating modes inside the waveguides that form the MZI arms. If Δn_e is the difference of the effective indices between the two arms due to V_π, then the phase difference between the arms is $(2\pi L\ \Delta n_e / \lambda_o)$. The MZI arm length that is sufficient for this phase difference to be equal to π, is denoted by L_π, and is found from $L_\pi = \lambda_o/(2\ \Delta n_e)$. It is always required to have as small switching voltage and arm length as possible. However, practically as one of these two parameter decreases, the other increases. Obviously, this is a consequence of the need for more voltage in order to increase Δn_e.

Other metrics include, of course, the maximum frequency of modulation, denoted here by f_{3dB}, which is also called the switching speed. Also, two extra metrics are used to show the efficiency of the modulator in terms of the optical losses. Those are the insertion loss (IL) and the extinction ratio (ER). If the input optical intensity is I_o, the maximum output optical intensity is I_H and the minimum is I_L, then IL = 10 log (I_o/ I_H) and ER = 10 log (I_H/ I_L).

III. Modal Analysis

The waveguide height is chosen to be 0.1 µm in order to minimize the scattering losses. The scattering losses are due to

rough waveguide sides that are created by etching. Lower sides, decrease the interaction between the mode and the rough walls and hence the scattering losses. This waveguide is single mode as long as the width is below 750 nm, which is the width used in this work. The maximum possible width gives the maximum confinement factor which means maximum interaction between the laser power and the moving charges. The intensity distribution of the fundamental quasi transverse-electric (TE) mode is shown in Fig. 2.

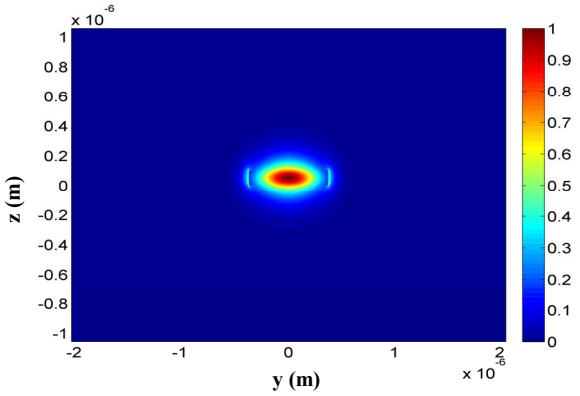

Fig. 2. The intensity distribution of the fundamental mode in the wavegudie. The color bar to the right shows the intensity level.

IV. Electrode Position

The left electrode is connected to ground while the right is connected to the voltage source responsible for the modulating signal. In our simulations, the electrodes are moved around the waveguide by changing 'y_o' and 'z_o'. As 'z_o' increases, the right electrode moves farther from the core up and the left electrode moves farther down. As 'y_o' increases, the right electrode moves farther to the right while the left electrode moves farther to the left. The minimum y-distance in this study is 100 nm. This is to avoid massive optical absorption losses and plasmonic modes. Besides, the left electrode is not allowed right under the core because this imposes a fabrication difficulty that contradicts with simplicity of fabrication which is one of the main objectives of this design for future implementation, as mentioned earlier. The applied voltage is in the range between -20 Volt and +20 Volt. The positive voltage pushes the majority carriers, the holes, away from the right electrode causing depletion. The negative voltage attracts the holes toward the right electrode causing accumulation. This charge study is conducted using DEVICE. The change of the effective refractive index at any applied voltage w.r.t. the case with zero voltage is shown in Fig. 3, Fig. 4, Fig. 5, Fig. 6, Fig. 7, and Fig. 8 for z_o= 0, z_o = 100 nm, z_o = 200 nm, z_o = 300 nm, z_o = 400 nm and z_o = 500 nm respectively.

Then, the charge distribution is exported from DEVICE to MODE to find the effective index and the absorption losses due to the carriers and the metallic electrodes. The maximum difference in the effective index is used to calculate the corresponding L_π. The scattering loss is taken safely as 1 dB/cm [19]. Hence, the insertion loss is calculated, excluding other loss mechanisms [20] such as fiber-grating coupler losses. The corresponding results are shown in Fig. 9 and Fig. 10.

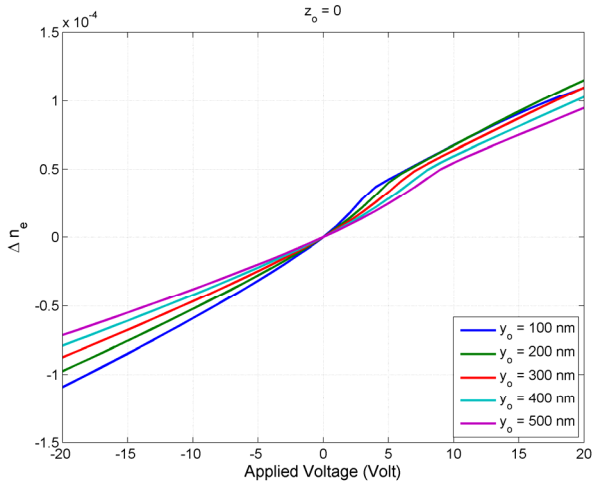

Fig. 3. The change of the effective index versus the applied voltage for different y_o at z_o = 0.

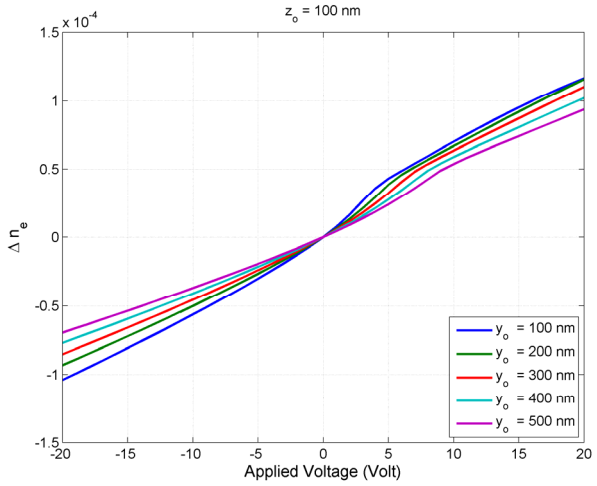

Fig. 4. The change of the effective index versus the applied voltage for different y_o at z_o = 100 nm.

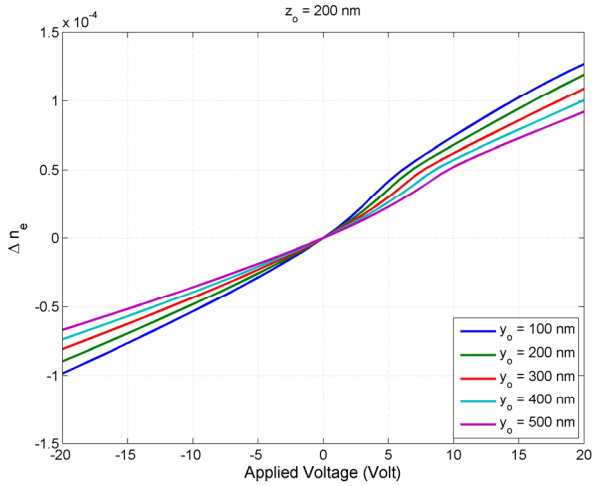

Fig. 5. The change of the effective index versus the applied voltage for different y_o at z_o = 200 nm.

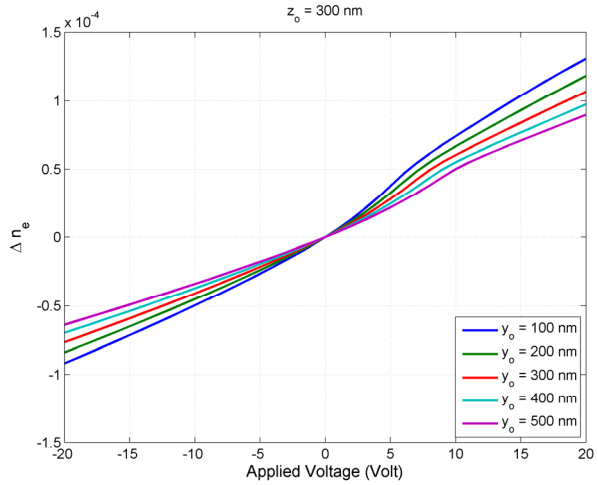

Fig. 6. The change of the effective index versus the applied voltage for different y_o at z_o = 300 nm.

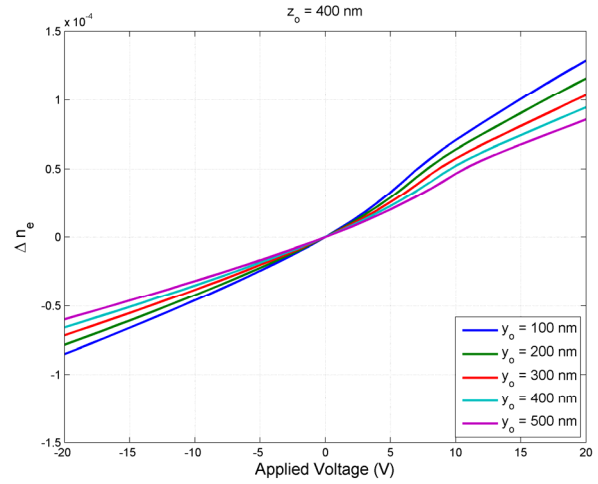

Fig. 7. The change of the effective index versus the applied voltage for different y_o at z_o = 400 nm.

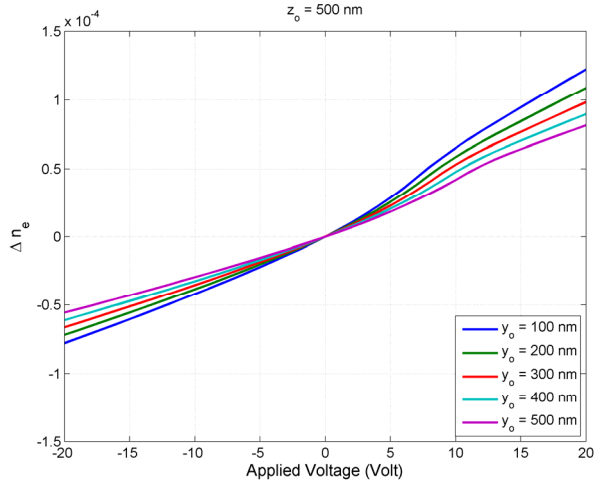

Fig. 8. The change of the effective index versus the applied voltage for different y_o at z_o = 500 nm.

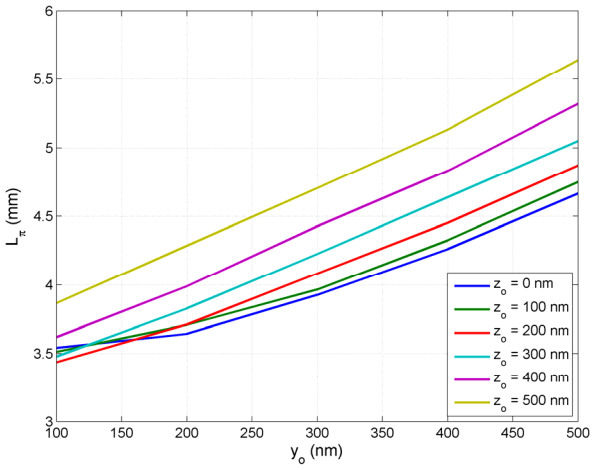

Fig. 9. The length of the modulator versus y_o for different z_o values.

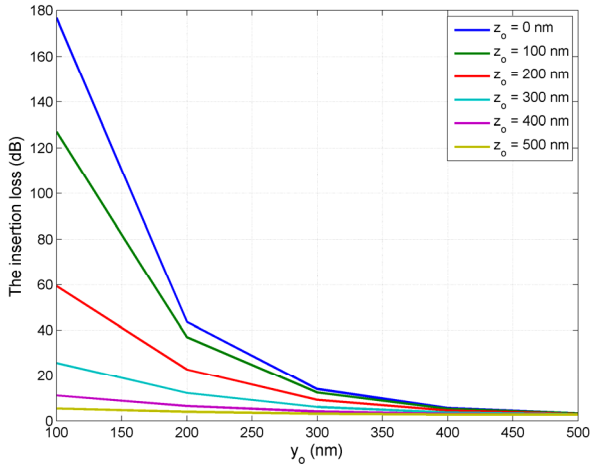

Fig. 10. The insertion loss of the modulator versus y_o for different z_o values.

Clearly, the closer the electrodes get to the core, the higher the absorption loss is. On the contrary, with closer electrodes, a smaller part of the voltage drop is given to the oxide and a larger part to the silicon core which leads to a stronger effective index change and a shorter required length. Therefore, a trade-off exists between the device length and losses.

In Fig. 9, it is noticeable that at y_o = 100 nm, the value of L_π is slightly larger at at z_o = 0 than that at z_o = 100 nm which is in turn is larger than that at z_o = 300 nm. This could be interpreted as follows. When z_o = 0, the long dimension of the electrode does not seem to be contributing to the electric field that moves the free carriers. This is because the electrodes are in plane with the core. At z_o = 100 nm, the long dimension starts to come in play which means more change to the carrier concentration which leads to a larger effective index change and hence a smaller L_π. Apparently, as z_o increases, there is no more contribution from the long dimension of the electrode.

That is why the effect of increasing z_o is simply increasing L_π. At y_o >150, the effect of z_o on L_π is monotonic. This means that the large dimension of the electrode has a minimal effect. Therefore, at y_o = 100 nm we expect the best effect of the electrode large dimension and then we choose z_o as explained shortly.

For a competitive performance in comparison with the modulators listed in, [4], [13] and [21], we study here the conditions for IL ~ 5 dB. We find that the shortest L_π under this condition is 3.86 mm with IL = 5.4 dB at z_o = 500 nm and y_o = 100 nm. The corresponding extinction ratio is ER = 28 dB. This strong ER makes this modulator a very good candidate for wavelength-division-multiplexing (WDM) applications [9]. The best length found under the same condition for a planar modulator, i.e. with the electrodes at the same horizontal level with the core or equivalently z_o = 0, is at y_o = 400 nm with L_π = 4.26 mm and IL = 5.6 dB. This means that the vertical misalignment of the electrode positions gives advantageous numbers regarding the size of the device since the length is 0.4 mm shorter and the width is 600 nm shorter too. This means a higher density of device integration.

For the device with z_o = 500 nm and y_o = 100 nm, the hole distributions over the cross section of the waveguide core are shown in Fig. 11 for 20 volt and Fig. 12 for -20 volt, respectively.

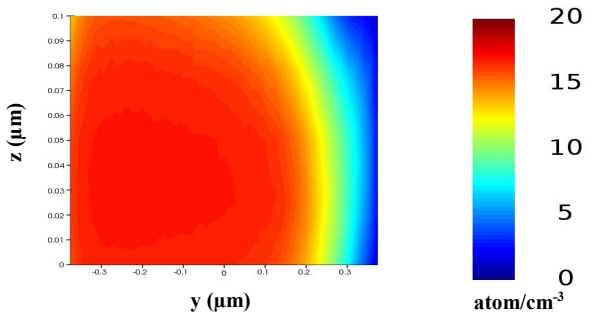

Fig. 11. The hole distribution over the core when the applied voltage equals 20 volt for the device with y_o =100 nm at z_o = 500 nm. The color bar shows the log scale.

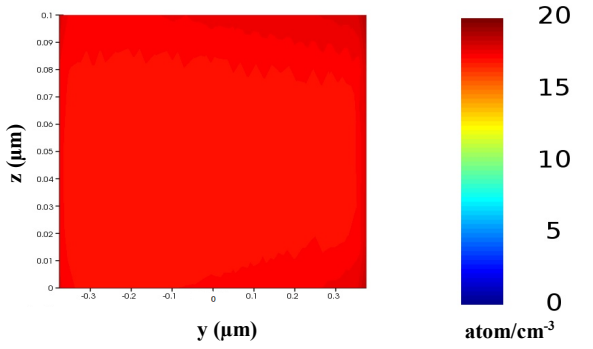

Fig. 12. The hole distribution over the core when the applied voltage equals -20 volt for the device with y_o =100 nm at z_o = 500 nm. The color bar shows the log scale.

We calculated the integration of the density of holes and the density of electrons over the waveguide cross section and plotted the results versus the applied voltage in Fig. 13. As the applied voltage increases, the number of holes decreases because of the depletion process, while the number of electrons increases, and vice versa.

The frequency response is tested using DEVICE and MODE. The modulating voltage takes the form of an impulse that changes from -20 volt to 20 volt within a time of 10 ps. The calculated effective index shows a corresponding change from its minimum value to its maximum during the same time as shown in Fig. 14. The change of the effective refractive index follows closely the voltage change with negligible delay in time. This means that this device is suitable for modulation at 100 Gbps. The effective index though, changes nonlinearly with voltage since the charge accumulation and depletion is not a linear phenomenon in voltage. Therefore, the sensitivity of the effective index to the applied voltage changes from one voltage value to another.

If compared to the devices studied in [4], [13] and [21], the proposed device shows better IL and ER than most of the listed devices. Because of the large oxide thickness between silicon and gold, the capacitance is very small which enables the device to operate at 100 Gbps which is much faster than the devices reported in [4], [13] or [21]. More importantly, which is the main motivation for this work, this device design enables future easier fabrication using a relatively inexpensive technology, because of its simple doping profile and geometry. In many devices [4], the electrodes require two different masks for fabrication like the device demonstrated here. But in other devices, they can be created using one mask only. However, this device saves many other steps needed for different doping concentrations. Using a push-pull technique, the required voltage of operation is +20 volt for one arm of the MZI and -20 volt for the other. This is also in the same range as in many devices from the same category [21]. If compared to other works using other platforms as in [22], the proposed modulator is, again, much simpler in fabrication as it best utilizes the mature and standard complementary metal-oxide-semiconductor (CMOS) technology. And along with the small size of this modulator, upon future fabrication, the production cost will be very competitive.

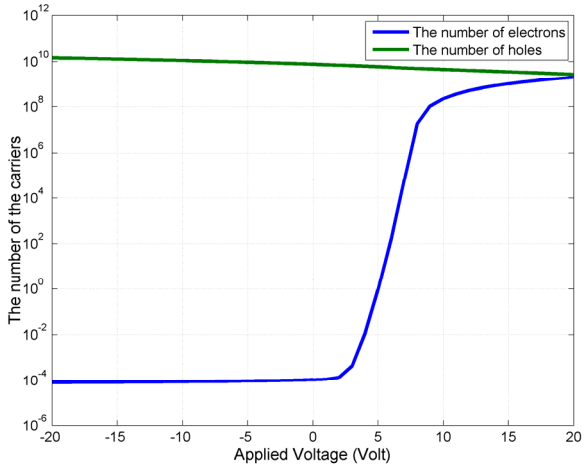

Fig. 13. The number of holes and the number of electrons versus the applied voltage.

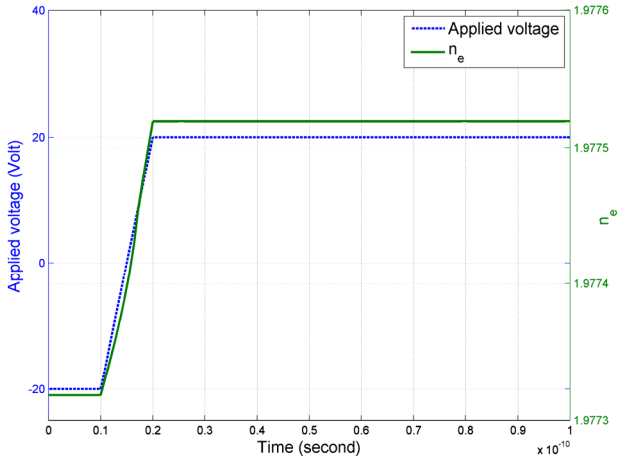

Fig. 14. The transient response of the modulator. The applied electric voltage changes from -20 volt to 20 volt in 10 ps and the effective index follows very closely.

V. CONCLUSION

An electro-optic modulator is proposed. This modulator is based on silicon-on-insulator technology with the modulation carried out using carrier depletion and accumulation. The capacitor based performance guarantees a very high modulation speed of 100 Gbps. The metallic electrodes are positioned such that the total insertion loss is only 5.4 dB and the total size of the modulator is much smaller than a planar modulator where the electrodes are positioned on the same horizontal level of the waveguide core. The extinction ratio of 28 dB makes this modulator suitable for practical WDM communications applications.

VI. REFERENCES

[1] V. Passaro, F. Dell'Olio, B. Casamassima and F. De Leonardis,"Guided-wave optical biosensors," Sensors, vol. 7, pp. 508-536, 2007.

[2] J. T. Robinson, L. Chen and M. Lipson,"On-chip gas detection in silicon optical waveguides," Optics Express, vol. 16, pp.4296-4301, 2008.

[3] E. Agrill et al, "Roadmap of optical communications," Journal of Optics, vol. 18, no. 6, 2016.

[4] G. Reed et al,"Recent breakthroughs in carrier depletion based silicon optical modulators," Nabophotonics, vol. 3, pp. 229-245, 2014.

[5] M. Gad, D. Yevick and P. E. Jessop, "Tunable polymer/silcion over insulator ring resonators," Optical Engineering, vol. 47, no. 12, 2007.

[6] G. Keiser, Optical fiber communications, 2nd ed, McGrew-Hill Inc., 1991, pp. 11.

[7] Y. Chen et al, "A 25 Gb/s hybrid integrated silicon photonic transceiver in 28 nm CMOSand SOI," ISSCC 2015, DOI: 10.1109/ISSCC.2015.7063096.

[8] Y. Vlasov and S. J. McNab, "Losses in single-mode silicon-on-onsulator strip waveguides and bends," Optics Express, vol. 12, pp. 1622-1631, 2004.

[9] M. Gad, J. Ackert, D. Yevick, L. Chrostowski and P. E. Jessop, "Ring resonator wavelength division multiplexing interleaver," Journal of Lightwave Technology, vol. 29, pp. 2102-2108, 12, 2011.

[10] B. Troia, V. M. N. Passaro, "Investigation of a novel silicon-on-insulator Rib-Slot photonic sensor based on the vernier effect and opertating at 3.8 µm," Journal of the European Optical Society, vol. 9, ISSN 1990-2573 - 2014.

[11] M. Gad, A. Zaki and Y. M. Sabry, "Silicon photonic mid-infrared grating coupler based on silicon-on-insulator technology," NRSC 2017, pp. 400-406.

[12] Q. Xu, B. Schmidt, S. Pradhan and M. Lipson, "Micrometre-scale silicon electro-optic modulator," Nature, vol. 435, pp. 325–327, 2005.

[13] G. T. Reed, G. Mashanovich, F. Y. Gardes and D. J. Thomson, "Silicon optical modulators," Nature Photonics, vol. 4, pp.518-526, 2010.

[14] R. Soref and B. Bennett, "Electrooptical effects in silicon," IEEE Journal of Quantum Electronics, vol. 23, pp,123–129, 1987.

[15] C. A. Barrios and M. Lipson, "Modeling and analysis of high-speed electro-optic modulation in high confinement silicon waveguides using metal-oxide-semiconductor configuration," Journal of Applied Physics, vol. 96, pp. 6008-6015, 2004.

[16] www.Lumerical.com

[17] E. D. Palik, Handbook of Optical Constants of Solids, Academic Press. 1998, pp. 286, 571 and 719.

[18] S. M. Sze, Physics of Semicondictor Devices, 2nd ed, John Wiley and Sons, 1981, pp. 27-38.

[19] T. Horikawa, D. Shimura and T. Mogami, "Low-loss silicon wire waveguides for optical integrated circuits," MRS Communications,vol. 6, pp. 9-15, 2016.

[20] F. Y. Gardes, D. J. Thomson, N. G. Emerson and G. T. Reed, "40 Gb/s silicon photonics modulator for TE and TM polarisations," Optics Express, vol. 19, pp.11804-11814, 2011.

[21] X. Xiao et al, "High-speed, low-loss silicon Mach–Zehnder modulators with doping optimization," Optics Express, vol. 21, pp. 4116-4125, 2013.

[22] C. Wang, M. Zhang, B. Stern, M. Lipson and M. Loncar, "Nanophotonic lithium niobate electro-optic modulators," Optics Express, vol. 26, pp. 1547-1555, 2018.